# Domain Wall Based Spin-Hall Nano-Oscillators

N. Sato,[1] K. Schultheiss,[1] L. Körber,[1,2] N. Puwenberg,[3] T. Mühl,[3] A. A. Awad,[4] S. S. P. K. Arekapudi,[5] O. Hellwig,[1,5] J. Fassbender,[1,2] and H. Schultheiss[1,2,*]

[1]*Helmholtz-Zentrum Dresden–Rossendorf, Institut für Ionenstrahlphysik und Materialforschung, D-01328 Dresden, Germany*

[2]*Technische Universität Dresden, 01062 Dresden, Germany*

[3]*Leibniz Institute for Solid State and Materials Research (IFW) Dresden, 01069 Dresden, Germany*

[4]*Department of Physics, University of Gothenburg, 412 96 Gothenburg, Sweden*

[5]*Institut für Physik, Technische Universität Chemnitz, D-09107 Chemnitz, Germany*

(Received 20 February 2019; published 2 August 2019)

In the last decade, two revolutionary concepts in nanomagnetism emerged from research for storage technologies and advanced information processing. The first suggests the use of magnetic domain walls in ferromagnetic nanowires to permanently store information in domain-wall racetrack memories. The second proposes a hardware realization of neuromorphic computing in nanomagnets using nonlinear magnetic oscillations in the gigahertz range. Both ideas originate from the transfer of angular momentum from conduction electrons to localized spins in ferromagnets, either to push data encoded in domain walls along nanowires or to sustain magnetic oscillations in artificial neurones. Even though both concepts share a common ground, they live on very different timescales which rendered them incompatible so far. Here, we bridge both ideas by demonstrating the excitation of magnetic auto-oscillations inside nanoscale domain walls using pure spin currents. This Letter will shed light on the current characteristic and spatial distribution of the excited auto-oscillations.

DOI: 10.1103/PhysRevLett.123.057204

The spin-transfer-torque (STT) effect discovered in 1996 by Slonczewski and Berger [1,2] allows the manipulation of localized magnetic moments in a ferromagnet by the transfer of spin angular momentum from spin polarized conduction electrons. The direction of the magnetization can either be switched permanently [3–5] or can be forced to oscillate at radio frequencies [6]. Quite soon thereafter it was recognized that a charge current in a ferromagnet, which is intrinsically spin polarized, can move magnetic domain walls (DWs) in nanowires [7]. This gave rise to the idea of the magnetic racetrack memory [8] and, quite recently, current-induced skyrmion motion [9–11]. While these schemes target nonvolatile, long term data storage, the STT effect in spin-torque nano-oscillators can be exploited to drive magnetic auto-oscillations [6,12] and, eventually, to radiate spin waves [13] by compensating the intrinsic magnetic damping. Another leap was the development of spin-Hall nano-oscillators (SHNO) [14,15] in which pure spin currents are generated via the spin-Hall effect (SHE) [16–19] and by which even propagating spin waves are excited [20,21]. This puts SHNOs at the heart of magnonics [22–24] which proposes a novel type of low energy, non-Boolean computing based on magnons, the quanta of spin waves, as carriers of information [25], or even neuromorphic computing [26,27] based on the nonlinear character of magnonic auto-oscillations. In a previous work, we demonstrated that DWs can channel magnons in an effective magnetic potential well [28]. This raised the question of whether or not a magnetic DW can potentially be a self-organized, movable SHNO, as was proposed by micromagnetic simulations for an out-of-plane system [29].

In order for the STT effect to counteract the intrinsic magnetic damping, the magnetization $\vec{\mathbf{M}}$ has to have a component antiparallel to the polarization $\vec{\mathbf{P}}$ of the injected spin current $I_s$ with density $\vec{\mathbf{J}}_s$. Because of spin-dependent scattering associated with the SHE, a charge current $I_c$ with density $\vec{\mathbf{J}}_c$ flowing in a heavy metal is converted into a transverse pure spin current with $\vec{\mathbf{J}}_s \perp \vec{\mathbf{J}}_c \perp \vec{\mathbf{P}}$ [Fig. 1(a)]. In a conventional nanowire, therefore, an external magnetic field is needed to overcome the shape anisotropy and to align $\vec{\mathbf{M}} \perp \vec{\mathbf{J}}_c$ [30]. Additionally, $I_s$ needs to be high enough to exert sufficient torque and compensate the magnetic damping. Typically, this is achieved by lithographically patterning devices with active areas of only few 10–100 nm [31].

However, the sizes are limited by lithography and the position of the active area is fixed. To overcome these limitations, we investigated the excitation of auto-oscillations inside magnetic DWs which bring multiple benefits: they can be created and destroyed dynamically, are very small, inherently exhibit $\vec{\mathbf{M}} \perp \vec{\mathbf{J}}_c$, and can easily be moved by electric currents, lasers, and small magnetic

 © 2019 American Physical Society

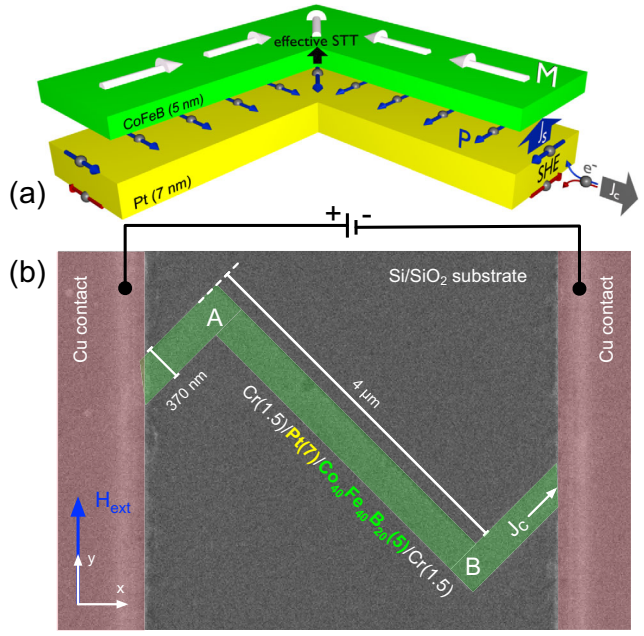


FIG. 1. (a) Schematic of a SHNO based on a domain wall. The functional layers of Pt and $Co_{40}Fe_{40}B_{20}$ are separated only for illustration purposes. (b) SEM image of the investigated 370-nm wide nanowire that exhibits two 90° bends at positions *A* and *B* and is connected to a current source by two Cu contacts.

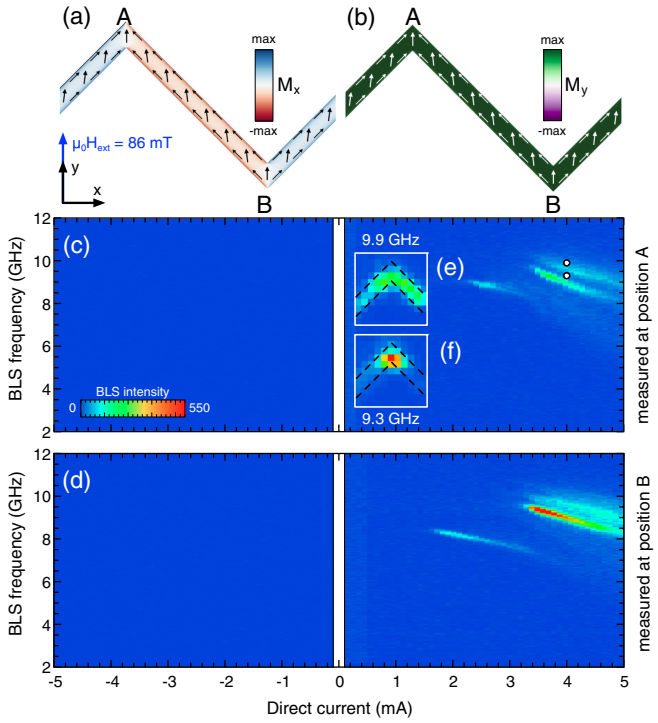


FIG. 2. (a),(b) Micromagnetic simulation of (a) the *x* and (b) the *y* component of the equilibrium magnetization under an applied field of $\mu_0 H_{ext} = 86$ mT. (c),(d) BLS spectra recorded at positions *A* and *B*, respectively, with an external field of $\mu_0 H_{ext} = 86$ mT covering the current range between −0.1 to −5 mA and 0.1 to 5 mA, respectively. Insets (e) and (f) show the two-dimensional intensity distributions of auto-oscillations excited at 9.3 and 9.9 GHz with $I_c = 4$ mA. Please note that the dc sweeps and the two-dimensional maps were recorded on different samples. Because of minor differences in the lithographic patterning of the two samples, there is a slight mismatch in the auto-oscillation frequencies recorded at 4 mA as indicated by the two white dot markers.

fields. This Letter demonstrates the possibility to drive strongly localized magnon auto-oscillations inside 90° DWs before they are moved by current-induced DW motion.

At the heart of any SHNO is a bilayer stack of a heavy metal in direct contact to a ferromagnet (Fig. 1). In our experiments, we use $Cr(1.5)/Pt(7)/Co_{40}Fe_{40}B_{20}(5)/Cr(1.5)$ multilayers, with Pt and CoFeB as the functional materials. To reproducibly control the formation of a DW, we use electron beam lithography to pattern the functional stack to a 370-nm wide zigzag shaped nanowire with two 90° bends, as highlighted in light green in the scanning electron microscopy (SEM) image in Fig. 1(b). Two $Ta(5)/Cu(150)/Ta(5)$ contacts allow for the application of a direct charge current $I_c$ with density $\vec{\mathbf{J}}_c$. All thicknesses are given in nanometers. As is depicted in Fig. 1(a), the SHE in Pt converts $\vec{\mathbf{J}}_c$ into a transverse pure spin current $I_s$ with density $\vec{\mathbf{J}}_s$ and polarity $\vec{\mathbf{P}}$. For a parallel (antiparallel) orientation of $\vec{\mathbf{P}}$ and $\vec{\mathbf{M}}$, the STT leads to an increased (decreased) effective damping of the magnetization dynamics in the CoFeB. In order to define the magnetic ground state, the sample can be saturated by an external magnetic field $\vec{\mathbf{H}}_{ext}$ applied along the *y* axis.

First, we saturated the structure at $\mu_0 H_{ext} = 500$ mT and then reduced the value to $\mu_0 H_{ext} = 86$ mT. In Figs. 2(a) and 2(b), we plot the simulated *x* and *y* component of the magnetization in the resulting equilibrium state which was obtained using the code from the GPU-based finite-difference micromagnetic package MUMAX3 [32]. The material parameters used in the simulations include the saturation magnetization $\mu_0 M_s = 1.28$ T, exchange stiffness of $A_{ex} = 20$ pJ/m, and damping parameter $\alpha = 0.001$. As can be seen from the $M_y$ component [Fig. 2(b)], the magnetization in the center of the nanowire width aligns along the external field. Only at the boundaries, the magnetic moments line up with the edges to reduce the demagnetization field, as evidenced by the nonvanishing $M_x$ component in Fig. 2(a). This state results in $\vec{\mathbf{M}} \perp \vec{\mathbf{J}}_c$ only inside the 90° bends at positions *A* and *B*. In the straight parts of the nanowire, $\vec{\mathbf{J}}_c$ flows at a 45° angle with respect to $\vec{\mathbf{M}}$, which strongly reduces the efficiency of the STT and, thus, the excitation of auto-oscillations.

To observe these auto-oscillations, we use space-resolved Brillouin light scattering (BLS) microscopy [33]. This technique relies on the inelastic scattering of a focused laser from magnetic oscillations. The inelastically

scattered light is then analyzed in a high-resolution interferometer, yielding a signal that is directly proportional to the local oscillation intensity.

In Figs. 2(c) and 2(d), we plot the BLS intensity that was measured at positions $A$ and $B$, respectively, as a function of the BLS frequency and the applied charge current which was swept consecutively from $-0.1$ to $-5$ mA and from 0.1 to 5 mA. For negative currents, no auto-oscillations are excited because $\vec{\mathbf{P}} \| \vec{\mathbf{M}}$ which leads to an increased effective damping. For positive currents, however, $\vec{\mathbf{P}}$ is antiparallel to $\vec{\mathbf{M}}$, and at $I_c > 2.2$ mA one auto-oscillation mode is detected at a frequency of about 9 GHz. For $I_c > 3.4$ mA, even two modes are observed, starting at 9.6 GHz and 10.2 GHz. All modes show a negative frequency shift with increasing $I_c$ which is expected for in-plane magnetized SHNOs [12] due to the increasing precession angle and subsequent nonlinear frequency shift.

In order to illustrate the spatial character of the excited auto-oscillations, we record two-dimensional maps of the intensity distribution at a fixed direct current of $I_c = 4$ mA and an external field of $\mu_0 H_{ext} = 86$ mT. At this specific current, two auto-oscillations are excited at 9.3 and 9.9 GHz. The spatial intensity distributions in Figs. 2(e) and 2(f) show a strong localization of the 9.3 GHz mode at the apex, whereas the mode at 9.9 GHz is much more diverged. The localization is related to the changing angle between $\vec{\mathbf{J}}_c$ and $\vec{\mathbf{M}}$ as well as the slightly increased current density at the 90° bends.

Up to now, we always applied an external magnetic field in order to drive auto-oscillations within the nanowire. In the next step, we prepared a magnetic transverse DW at the 90° bends. Therefore, we again saturated the nanowire at $\mu_0 H_{ext} = 500$ mT but then reduced the external magnetic field to zero. Figure 3(a) depicts the resulting remanent state of the nanowire as derived from micromagnetic simulations. The shape anisotropy directs the magnetization to align along the nanowire, which creates a head-to-head (tail-to-tail) DW at positions $A$ ($B$), respectively.

The domain configuration in the remanent state is also confirmed by magnetic force microscopy (MFM) in Fig. 3(b). Therefore, an external field of $\mu_0 H_{ext} = 500$ mT was applied and slowly reduced to zero before starting the MFM measurements. The measurements were performed in a Nanoscan high resolution magnetic force microscope in high vacuum using a high aspect ratio MFM probe (Team Nanotec HR-MFM45 with ML1 coating and a spring constant of 0.7 N/m). The local tip-sample distance was 82 nm. The bright (dark) contrast at position $A$ ($B$) in the $dF_z/dz$ signal confirms the formation of DWs where $F_z$ is the $z$ component of the magnetostatic tip-sample interaction.

In the straight parts of the nanowire, the charge current flows along the magnetization ($\vec{\mathbf{J}}_c \| \vec{\mathbf{M}}$) so that no auto-oscillations can be excited. Only inside the DWs at positions $A$ and $B$, the direct current and the magnetization

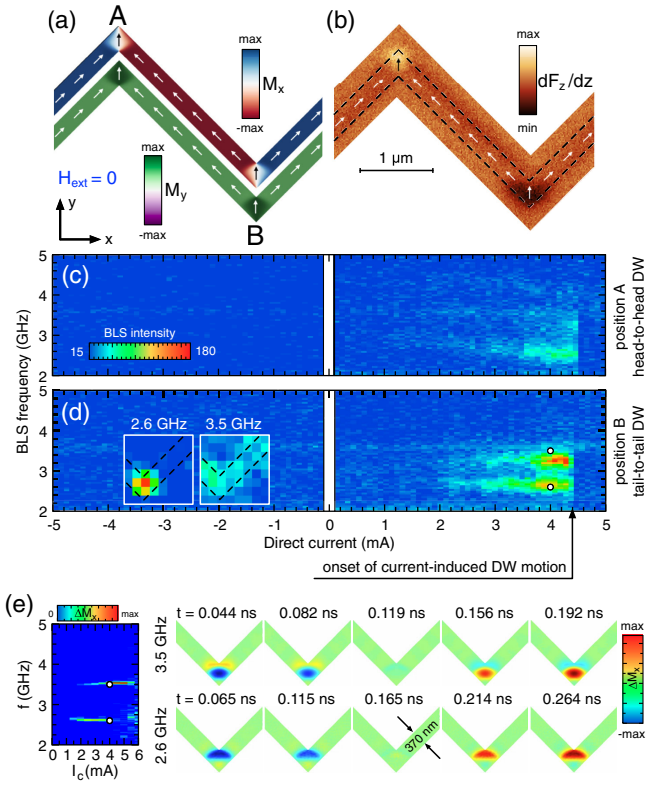


FIG. 3. (a) Micromagnetic simulation and (b) MFM measurement of the remanent magnetization after saturating the sample with $\mu_0 H_{ext} = 500$ mT and reducing the field back to zero. (c),(d) BLS spectra measured as a function of the applied $I_c$ on the DWs at positions $A$ and $B$, respectively. The direct current was swept from $-0.1$ to $-5$ mA and from 0.1 to 5 mA, respectively. In between the consecutive current sweeps, the sample was saturated to ensure the proper domain configuration. Insets in (d) show the two-dimensional BLS intensity distributions of auto-oscillations excited in the remanent state at 2.6 and 3.5 GHz for $I_c = 4$ mA. (e) Micromagnetic simulations of the current sweep (left) and the temporal evolution (right) of the amplitudes of the simulated auto-oscillation modes excited at 2.6 and 3.5 GHz for a half cycle with $I_c = 4$ mA.

are aligned perpendicularly so that we expect to observe auto-oscillations only in these narrow regions.

When we apply currents between $-0.1$ and $-5$ mA and measure the BLS intensities inside the DWs at positions $A$ and $B$ [see Figs. 3(c) and 3(d), respectively], we again see no auto-oscillations due to increased damping in this direction. For positive currents, however, we observe two auto-oscillation modes at 2.6 and 3.5 GHz. These modes do not show a pronounced negative frequency shift and one of them is in fact strongly localized to the DW, as is confirmed by spatially resolved BLS microscopy [see insets in Fig. 3(d)]. The experimental results are further corroborated by micromagnetic simulations in Fig. 3(e), which show the localization of both modes and a node in the dynamic magnetization profile of the higher frequency mode.

We ran the simulations of the auto-oscillation modes for a geometry with a lateral size of $4000 \times 3000 \times 5$ nm$^3$, and unit cell size $3.9 \times 3.9 \times 5$ nm$^3$. Absorbing boundary conditions in the form of a smooth increase of the damping profile are applied to the open edges of the nanowire to avoid artifacts from spin-wave reflection. The direct charge current transport was simulated using COMSOL Multiphysics using layer resistivities of 90 and 11.2 $\mu\Omega$ cm for CoFeB and Pt, respectively. The current profile and the Oersted field are then supplied to MUMAX3, taking into account a spin-Hall angle of $\theta_{SH} = 0.08$ and the calculated spatial distribution of the spin current polarization. All parameters were used according to previous studies of the same material system [34–37]. The auto-oscillation spectra were obtained by applying a fast Fourier transform (FFT) to the net $x$ component of the total magnetization, simulated over 100 ns. The spatial profiles of the auto-oscillation modes are constructed via an FFT for each simulation cell [38]. The auto-oscillation modes show very similar profiles and frequencies to the linear modes excited with a field pulse at zero current, in other words the DW auto-oscillations nucleate from linear modes, similar to the high frequency modes in other SHNOs [39].

We would like to stress the fact that for $I_c > 4.5$ mA the measured BLS intensity at positions $A$ and $B$ abruptly disappears. Indeed, this is still the case when we decrease the current again. Only a repeated saturation and relaxation of the sample, as described before, restores the auto-oscillations as shown in the Supplemental Material [40]. This illustrates that for $I_c > 4.5$ mA the DWs are removed from the apexes due to the current-induced DW motion. For lower currents, this motion is suppressed by the dipolar pinning of the DWs at the apexes. One can exploit this motion with a precise current pulse, e. g., to shift one DW from position $A$ to position $B$.

In conclusion, we have demonstrated that a pinned transversal DW is able to work as a nanosized spin-torque oscillator. Once prepared, this oscillator is able to perform at zero external magnetic field. Moreover, the auto-oscillations appear at current densities at which the current-induced DW motion does not yet set in. In other words, the DW oscillates at GHz frequencies before it moves. In principle, the ratio of these two thresholds can be tuned by changing the relative thicknesses or materials of the functional layers or by replacing the metallic ferromagnet with an insulating one. On the other hand, the combination of auto-oscillations and current-induced DW motion yields various possibilities for research in fundamental DW physics as well as for applications. One could think of using movable DW spin-torque oscillators in networks to achieve more flexibility in synchronization or frequency locking or even further advance concepts for magnetic racetrack memories or neuromorphic computing.

Financial support by the Deutsche Forschungsgemeinschaft within programme SCHU2922/1-1 is gratefully acknowledged. N. S. acknowledges funding from the Alexander von Humboldt Foundation. K. S. acknowledges funding from the Helmholtz Postdoc Programme. Samples were fabricated at the Nanofabrication Facilities (NanoFaRo) at the Institute of Ion Beam Physics and Materials Research at HZDR. We thank Dr. Ingolf Mönch for deposition of the Ta/Cu/Ta multilayer.

*h.schultheiss@hzdr.de

[1] J. C. Slonczewski, J. Magn. Magn. Mater. **159**, L1 (1996).
[2] L. Berger, Phys. Rev. B **54**, 9353 (1996).
[3] E. B. Myers, D. C. Ralph, J. A. Katine, R. N. Louie, and R. A. Buhrman, Science **285**, 867 (1999).
[4] J. E. Wegrowe, D. Kelly, Y. Jaccard, P. Guittienne, and J.-P. Ansermet, Europhys. Lett. **45**, 626 (1999).
[5] J. Z. Sun, J. Magn. Magn. Mater. **202**, 157 (1999).
[6] S. I. Kiselev, J. C. Sankey, I. N. Krivorotov, N. C. Emley, R. J. Schoelkopf, R. A. Buhrman, and D. C. Ralph, Nature (London) **425**, 380 (2003).
[7] G. Beach, M. Tsoi, and J. L. Erskine, J. Magn. Magn. Mater. **320**, 1272 (2008).
[8] S. S. P. Parkin, M. Hayashi, and L. Thomas, Science **320**, 190 (2008).
[9] T. H. R. Skyrme, Nucl. Phys. **31**, 556 (1962).
[10] S. Mühlbauer, B. Binz, F. Jonietz, C. Pfleiderer, A. Rosch, A. Neubauer, R. Georgii, and P. Böni, Science **323**, 915 (2009).
[11] A. Fert, V. Cros, and J. Sampaio, Nat. Nanotechnol. **8**, 152 (2013).
[12] A. N. Slavin and V. Tiberkevich, IEEE Trans. Magn. **45**, 1875 (2009).
[13] M. Madami, S. Bonetti, G. Consolo, S. Tacchi, G. Carlotti, G. Gubbiotti, F. B. Mancoff, M. A. Yar, and J. Åkerman, Nat. Nanotechnol. **6**, 635 (2011).
[14] V. E. Demidov, S. Urazhdin, H. Ulrichs, V. Tiberkevich, A. Slavin, D. Baither, G. Schmitz, and S. O. Demokritov, Nat. Mater. **11**, 1028 (2012).
[15] V. E. Demidov, S. Urazhdin, A. Zholud, A. V. Sadovnikov, and S. O. Demokritov, Appl. Phys. Lett. **105**, 172410 (2014).
[16] M. I. Dyakonov and V. I. Perel, Sov. Phys. JETP Lett. **13**, 467 (1971).
[17] J. E. Hirsch, Phys. Rev. Lett. **83**, 1834 (1999).
[18] K. Ando, S. Takahashi, K. Harii, K. Sasage, J. Ieda, S. Maekawa, and E. Saitoh, Phys. Rev. Lett. **101**, 036601 (2008).
[19] A. Hoffmann, IEEE Trans. Magn. **49**, 5172 (2013).
[20] V. E. Demidov, S. Urazhdin, R. Liu, B. Divinskiy, A. Telegin, and S. O. Demokritov, Nat. Commun. **7**, 10446 (2016).
[21] B. Divinskiy, V. E. Demidov, S. Urazhdin, R. Freeman, A. B. Rinkevich, and S. O. Demokritov, Adv. Mater. **30**, 1802837 (2018).
[22] S. Neusser and D. Grundler, Adv. Mater. **21**, 2927 (2009).
[23] V. V. Kruglyak, S. O. Demokritov, and D. Grundler, J. Phys. D **43**, 264001 (2010).
[24] B. Lenk, H. Ulrichs, F. Garbs, and M. Münzenberg, Phys. Rep. **507**, 107 (2011).

[25] A. V. Chumak, V. I. Vasyuchka, A. A. Serga, and B. Hillbrands, Nat. Phys. **11**, 453 (2015).
[26] N. Locatelli, V. Cros, and J. Grollier, Nat. Mater. **13**, 11 (2014).
[27] J. Torrejon *et al.*, Nature (London) **547**, 428 (2017).
[28] K. Wagner, A. Kákay, K. Schultheiss, A. Henschke, T. Sebastian, and H. Schultheiss, Nat. Nanotechnol. **11**, 432 (2016).
[29] A. Bisig, L. Heyne, O. Boulle, and M. Kläui, Appl. Phys. Lett. **95**, 162504 (2009).
[30] Z. Duan, A. Smith, L. Yang, B. Youngblood, J. Lindner, V. E. Demidov, S. O. Demokritov, and I. N. Krivorotov, Nat. Commun. **5**, 5616 (2014).
[31] P. Dürrenfeld, A. A. Awad, A. Houshang, R. K. Dumas, and J. Åkerman, Nanoscale **9**, 1285 (2017).
[32] A. Vansteenkiste, J. Leliaert, M. Dvornik, M. Helsen, F. Garcia-Sanchez, and B. Van Waeyenberge, AIP Adv. **4**, 107133 (2014).
[33] T. Sebastian, K. Schultheiss, B. Obry, B. Hillebrands, and H. Schultheiss, Front. Phys. **3**, 35 (2015).
[34] M. Ranjbar, P. Duerrenfeld, M. Haidar, E. Iacocca, M. Balinskiy, T. Q. Le *et al.* IEEE Magn. Lett. **5**, 3000504 (2014).
[35] S. Y. Jang, C. You, S. H. Lim, and S. R. Lee, J. Appl. Phys. **109**, 013901 (2011).
[36] T. Devolder, J.-V. Kim, L. Nistor, R. Sousa, B. Rodmacq, and B. Diény, J. Appl. Phys. **120**, 183902 (2016).
[37] A. A. Awad, P. Drrenfeld, A. Houshang, M. Dvornik, E. Iacocca, R. K. Dumas, and J. kerman, Nat. Phys. **13**, 292 (2017).
[38] R. D. McMichael and M. D. Stiles, J. Appl. Phys. **97**, 10J901 (2005).
[39] M. Dvornik, A. A. Awad, and J. Åkerman, Phys. Rev. Applied **9**, 014017 (2018).
[40] See Supplemental Material at http://link.aps.org/supplemental/10.1103/PhysRevLett.123.057204 for more details.